Real-space representation of the winding number for a one-dimensional chiral-symmetric topological insulator

Ling Lin,[1,2] Yongguan Ke,[1,*] and Chaohong Lee[1,2,†]

[1]*Guangdong Provincial Key Laboratory of Quantum Metrology and Sensing & School of Physics and Astronomy, Sun Yat-Sen University (Zhuhai Campus), Zhuhai 519082, China*

[2]*State Key Laboratory of Optoelectronic Materials and Technologies, Sun Yat-Sen University (Guangzhou Campus), Guangzhou 510275, China*

(Received 21 January 2021; accepted 9 June 2021; published 21 June 2021)

The winding number has been widely used as an invariant for diagnosing topological phases in one-dimensional chiral-symmetric systems. We put forward a real-space representation for the winding number. Remarkably, our method reproduces an exactly quantized winding number even in the presence of disorders that break translation symmetry but preserve chiral symmetry. We prove that our real-space representation of the winding number, the winding number defined through the twisted boundary condition, and the real-space winding number derived previously [Phys. Rev. Lett. **113**, 046802 (2014)], are equivalent in the thermodynamic limit at half-filling. Our method also works for the case of filling less than one half, where the winding number is not necessarily quantized. Around the disorder-induced topological phase transition, the real-space winding number has large fluctuations for different disordered samples, however, its average over an ensemble of disorder samples may well identify the topological phase transition. Besides, we show that our real-space winding number can be expressed as a Bott index, which has been used to represent the Chern number for two-dimensional systems.

DOI: 10.1103/PhysRevB.103.224208

I. INTRODUCTION

Topological states have attracted a tremendous amount of studies in various systems involving electrons, cold atoms, photons, etc. Most of the noninteracting topological states can be successfully explained by topological band theory [1] based on perfect translation symmetry [2–5]. The first well-known example is the integer quantum Hall effect [6], in which the quantized Hall conductivity is related to a topological TKNN invariant [7] defined with Bloch wave functions of filling bands. However, in reality, there always exists disorder that breaks translation symmetry and hence the consequent Bloch wave functions. It becomes problematic for the calculation of topological invariants with Bloch wave functions. Numerous topological states immune to disorder [8–15] indicate that the lack of Bloch wave functions should not be a hindrance for defining topological invariants.

To circumvent the absence of translation symmetry, one may consider a real-space representation of the topological invariants. One of the well-known examples is the real-space representation of the Chern number. The construction of real-space representation of the Chern number is through transforming the momentum-space formula to the real-space one [16–18], or considering a Bott index [19,20]. The real-space representation of the Chern number has been widely used in studying disorder effects in two-dimensional topological systems [21–24]. Another example is that the polarization in one dimension can be calculated in the real space as well via the projected position operator approach [25–28]. Recently, a real-space representation of the winding number is proposed for one-dimensional (1D) topological insulators with chiral symmetry [29], in which the momentum-space formula of the winding number is transformed to a real-space formula. Provided that disorder does not break the chiral symmetry, such a real-space representation of the winding number has been proved to be valid and widely used in exploring the topological Anderson insulator [30–33], and particularly, for detection of the winding number in experiment [34,35]. On the other hand, we note the momentum-space winding number for 1D systems can be written as the "skew" polarization [29,36], that is, the difference of polarizations (Berry phases) between two sublattices. As the usual polarization for 1D lattices can be obtained via the projected position operator in real space, *can we derive the real-space winding number in views of the skew polarization*?

In this paper we propose a real-space representation of the winding number for 1D chiral-symmetric topological insulators. We use the singular value decomposition (SVD) method to derive a formula for calculating the difference of polarization between two sublattices. Our formula can be written in the form of the Bott index [37,38], which produces a strictly quantized winding number. We prove that our formula is exactly equivalent to the momentum-space winding number in the presence of translation symmetry. We also prove that our real-space representation of the winding number, the winding number defined through the twisted boundary condition

*keyg@mail2.sysu.edu.cn
†lichaoh2@mail.sysu.edu.cn

(TBC), and the real-space winding number derived previously in Ref. [29], are equivalent in the thermodynamic limit at half-filling. Provided the chiral symmetry is preserved, our formula is self-averaging and satisfies the bulk-edge correspondence in the presence of disorder. We have verified numerically that our results are in agreement with the previous works [29,30] on the disordered model after averaging over many random realizations. However, our method gives exactly quantization of the winding number in each realization of disorder, in stark contrast to previous methods [29,30]. Away from topological transition points, our method has advantages over the previous method [29,30] for higher accuracy and less fluctuation. Furthermore, we show that our formula can work for the case of filling less than one half. Also, we find our real-space representation of the winding number in one dimension can be written as the Bott index [19,23], which was used to define the real-space representation of the Chern number in two dimensions.

The rest of this paper is organized as follows: In Sec. II we review the projected position operator approach, and show that it is related to the Wilson loop. In Sec. III we employ SVD for the chiral-symmetric Hamiltonian to obtain the flattened Hamiltonian, and then construct a real-space representation of the winding number. We will prove the equivalence of our real-space representation of the winding number and the twisted-boundary winding number. In Sec. IV we apply our arguments to a 1D toy model belonging to BDI classe. Finally, in Sec. V we make a summary and discussion.

II. BULK POLARIZATION AND PROJECTED POSITION OPERATOR

In this section we give a brief review on calculating the bulk polarization in the 1D system via the projected position operator.

First, we consider a finite 1D lattice with L cells under periodic boundary conditions. When translational symmetry is present, quasimomentum k becomes a good quantum number, and the Hamiltonian has a block-diagonal structure. The eigenstates are Bloch waves labeled by quasimomentum k. The basis of momentum space is the Fourier transform of real-space basis. In the following context we use $|l,\alpha\rangle$ to refer to the state that a particle is located at the αth sublattice (orbital) of the lth cell. Thus, the basis of momentum space reads

$$|k,\alpha\rangle = \frac{1}{\sqrt{L}}\sum_{l=1}^{L} e^{ikl}|l,\alpha\rangle, \tag{1}$$

and the Bloch waves can be written as the linear combinations of momentum basis

$$|\psi_{k,n}\rangle = \sum_{\alpha} u^{n}_{k,\alpha}|k,\alpha\rangle, \tag{2}$$

where n is the index of the band.

The bulk polarization can be calculated through the following formula [28]:

$$p = \frac{1}{2\pi i}\log\det \mathcal{W}_{k+2\pi\leftarrow k}, \tag{3}$$

where $\mathcal{W}_{k+2\pi\leftarrow k}$ is the so-called Wilson loop

$$\mathcal{W}_{k+2\pi\leftarrow k} = F_{k+2\pi-\delta k}F_{k+2\pi-2\delta k}\cdots F_k. \tag{4}$$

The matrix element of F_k is $(F_k)_{m,n} = \langle u^{m}_{k+\delta k}|u^{n}_{k}\rangle$, in which m,n are the indices of occupied bands. We will also use this notation in the following context.

Next, we show the Wilson loop can be derived from the projected position operator $P_{\rm occ}\mathcal{X}P_{\rm occ}$, where $P_{\rm occ} = \sum_{n=1}^{n_{\rm occ}}\sum_{k}|\psi_{n,k}\rangle\langle\psi_{n,k}|$ is the projector onto occupied bands, and $|\psi_{n,k}\rangle$ is the eigenstate of system at the nth band with quasimomentum k. A quantum-mechanical position operator [39] $\hat{\mathcal{X}} = \exp(i\delta k\hat{X})$, in which $\hat{X} = \sum_x x\hat{n}_x$ is the general position operator, is introduced for a lattice with a periodic boundary condition. Here $\delta k = 2\pi/L$ is the increment of discrete quasimomentum k. Note that operator $\mathcal{X}$ is actually the translation operator for quasimomentum k: $\mathcal{X}|k,\alpha\rangle = |k+\delta k,\alpha\rangle$. By expanding the expression of projected position operator, we have

$$\begin{aligned} P_{\rm occ}\mathcal{X}P_{\rm occ} &= \sum_{n,n'=1}^{n_{\rm occ}}\sum_{k,k'}|\psi_{n',k'}\rangle\langle\psi_{n',k'}|\mathcal{X}|\psi_{n,k}\rangle\langle\psi_{n,k}| \\ &= \sum_{n,n'=1}^{n_{\rm occ}}\sum_{k}\langle u^{n'}_{k+\delta k}|u^{n}_{k}\rangle|\psi_{n',k+\delta k}\rangle\langle\psi_{n,k}|, \end{aligned} \tag{5}$$

where we have used the relation [40,41]

$$\begin{aligned} \langle\psi_{n',k'}|\mathcal{X}|\psi_{n,k}\rangle &= \sum_{\alpha,\alpha'}\left(u^{n'}_{k',\alpha'}\right)^{*}u^{n}_{k,\alpha}\langle k',\alpha'|\mathcal{X}|k,\alpha\rangle \\ &= \sum_{\alpha,\alpha'}\left(u^{n'}_{k',\alpha'}\right)^{*}u^{n}_{k,\alpha}\langle k',\alpha'|k+\delta k,\alpha\rangle \\ &= \sum_{\alpha,\alpha'}\delta_{k',k+\delta k}\delta_{\alpha,\alpha'}\left(u^{n'}_{k',\alpha'}\right)^{*}u^{n}_{k,\alpha} \\ &= \delta_{k',k+\delta k}\langle u^{n'}_{k'}|u^{n}_{k}\rangle. \end{aligned} \tag{6}$$

Then we seek the eigenvalues of the projected position operator (5). Assuming its eigenstates are the superposition of occupied Bloch states $|\Psi\rangle = \sum_{k,n}\Psi_{n,k}|\psi_{n,k}\rangle$, the eigenvalue problem reads

$$P_{\rm occ}\mathcal{X}P_{\rm occ}|\Psi\rangle = \lambda|\Psi\rangle. \tag{7}$$

Combining Eqs. (5) and (7), we obtain the following iterative relation:

$$\sum_{n=1}^{n_{\rm occ}}\langle u^{n'}_{k+\delta k}|u^{n}_{k}\rangle\Psi_{n,k} = \lambda\Psi_{n',k+\delta k}, \tag{8}$$

which can be further written in a more compact form

$$F_k\Psi_k = \lambda\Psi_{k+\delta k}, \tag{9}$$

where $\Psi_k = (\Psi_{1,k},\Psi_{2,k},\ldots,\Psi_{n_{\rm occ},k})^{\rm T}$, $[F_k]_{n',n} = \langle u^{n'}_{k+\delta k}|u^{n}_{k}\rangle$. Repeating the iterative relation for L times, we have

$$\mathcal{W}_{k+2\pi\leftarrow k}\Psi_k = \lambda^{L}\Psi_k, \tag{10}$$

which reveals that the Wilson loop is related to the eigenvalues of the projected position operator. We may obtain the bulk polarization directly through the projected position operator. In fact, the eigenstates of the projected position operator are

Wannier states, while its eigenvalues are center of mass of Wannier states [25–27].

To summarize, one may obtain the polarization from projected position operators directly in real space. This is beneficial for investigating the disorder system since the translation symmetry is broken and the Wilson loop method Eq. (3) is not applicable.

III. WINDING NUMBER OF THE 1D CHIRAL-SYMMETRIC TOPOLOGICAL INSULATOR

A. Chiral-symmetric system and singular-value decomposition

In this section we shall first review some properties of the chiral-symmetric system. Due to the special form of the chiral-symmetric Hamiltonian, we will introduce the singular value decomposition (SVD) for the Hamiltonian and construct a real-space representation of the winding number.

A lattice with chiral symmetry can be classified into two kinds of sublattices, namely A and B. Thus, the chiral symmetry is also called the sublattice symmetry. The Hilbert space of the system can be written as the direct sum of the two subspaces $\mathcal{H} = \mathcal{H}_A \oplus \mathcal{H}_B$. The chiral symmetry manifests that $\Gamma H \Gamma = -H$, where

$$\Gamma = \sum_{l,\alpha\in A} |l,\alpha\rangle\langle l,\alpha| - \sum_{l,\beta\in B} |l,\beta\rangle\langle l,\beta|. \tag{11}$$

In the canonical representation, where the chiral operator Γ is diagonal, the Hamiltonian has the following structure:

$$H = \begin{pmatrix} 0 & h \\ h^\dagger & 0 \end{pmatrix}, \tag{12}$$

where h is a $L_A \times L_B$ matrix. Here L_A and L_B are, respectively, the total numbers of A and B sublattices. By decomposing the eigenstates into two sectors $|\psi_n\rangle = (\psi_n^A, \psi_n^B)^T$, the eigenvalue equation $H|\psi_n\rangle = E_n|\psi_n\rangle$ leads to the coupled equations

$$\begin{aligned} h\psi_n^B &= E\psi_n^A, \\ h^\dagger\psi_n^A &= E\psi_n^B, \end{aligned} \tag{13}$$

which can be further written as

$$\begin{aligned} (hh^\dagger)\psi_n^A &= E^2\psi_n^A, \\ (h^\dagger h)\psi_n^B &= E^2\psi_n^B. \end{aligned} \tag{14}$$

Now we may obtain ψ_n^A and ψ_n^B by calculating the eigenvectors of $hh^\dagger$ and $h^\dagger h$, respectively. Note that both $(\psi_n^A, \pm\psi_n^B)^T$ are the eigenvectors of Hamiltonian (12), and they have opposite eigenenergies. This is a consequence of the chiral symmetry.

The expression of Eq. (14) reminds us of the singular value decomposition (SVD). We can make the SVD for the off-diagonal block $h = U_A \Sigma U_B^{-1}$, in which U_A and U_B are both unitary matrices, and Σ is a diagonal matrix. The diagonal elements of Σ are called singular values. We note that

$$\begin{aligned} U_A^{-1} hh^\dagger U_A &= \Sigma^2, \\ U_B^{-1} h^\dagger h U_B &= \Sigma^2, \end{aligned} \tag{15}$$

which reveals that U_A and U_B, respectively, diagonalize $hh^\dagger$ and $h^\dagger h$. Therefore, the singular values are identified as the non-negative eigenenergies of the system. The column of unitary matrices U_A and U_B are, respectively, the eigenvectors ψ_n^A and ψ_n^B (up to a normalization factor $1/\sqrt{2}$). We have not assumed the numbers of the two kinds of sublattices L_A, L_B in the above derivation. Actually, L_A and L_B can be different, and the matrix h is not necessarily squared. If $L_A \neq L_B$, there must be at least $|L_A - L_B|$ zero singular values. However, throughout this paper, we only consider the numbers of A and B sublattices that are equal. More precisely, we are interested in the situation where h is not singular. This further requires the system to be gapped at $E = 0$.

When all singular values are nonzero, one may deform the singular values to arbitrary positive values and still maintain the same eigenstates. Hence, it is convenient to set Σ to be identity. We denote the new Hamiltonian as

$$Q = \begin{pmatrix} 0 & q \\ q^{-1} & 0 \end{pmatrix}, \tag{16}$$

where $q = U_A U_B^{-1}$ is a unitary matrix. Now the energy spectrum of the Hamiltonian becomes completely flat and only takes values of $+1$ and -1. Q is called the flattened Hamiltonian [36]. Later we will see the SVD is convenient for calculating and understanding the winding number.

B. Winding number in momentum space

When translation symmetry is present, we can work in momentum space by introducing the Fourier transformation

$$|k,\alpha\rangle = \int \frac{dk}{2\pi} \exp(ikl)|l,\alpha\rangle.$$

Then we can block diagonalize the flattened Hamiltonian (16) as

$$Q(k) = \begin{pmatrix} 0 & q(k) \\ q(k)^{-1} & 0 \end{pmatrix}. \tag{17}$$

The eigenstates can be written as $|\psi_{n,k}\rangle = \sum_\alpha u_{n,k}^\alpha |k,\alpha\rangle$. There is a map from Brillouin zone to the unitary matrices $q(k)$. The map is classified by the first homotopy group $\pi_1[U(n)] \cong \mathbb{Z}$ and characterized by the winding number [36,42]. The winding number in 1D can be calculated via [36,42]

$$\nu = \frac{i}{2\pi}\int_{-\pi}^{\pi} dk \mathrm{Tr}\big[q(k)^{-1}\partial_k q(k)\big]. \tag{18}$$

By inserting $q(k) = U_A(k)U_B^{-1}(k)$ introduced in a previous subsection into Eq. (18), we find

$$\begin{aligned} \nu = &\frac{i}{2\pi}\int_{-\pi}^{\pi} dk \mathrm{Tr}\big[U_A(k)^{-1}\partial_k U_A(k)\big] \\ &-\frac{i}{2\pi}\int_{-\pi}^{\pi} dk \mathrm{Tr}\big[U_B(k)^{-1}\partial_k U_B(k)\big], \end{aligned} \tag{19}$$

where we have used a fact that $\mathrm{Tr}(U_q^{-1}\partial_q U_q) = -\mathrm{Tr}(U_q\partial_q U_q^{-1})$ when U_q is a unitary matrix. As mentioned above, the column of unitary matrix $U_\sigma(k)$ is the eigenvector $u_{n,k}^\sigma$ ($\sigma = A, B$) up to a normalization factor. One can find that Eq. (19) is exactly the "skew" polarization. The above expression can be considered as the difference of the polarization between two sublattices. In other words, the winding number (divided by 2) measures the difference

of polarization between A and B sublattices. In addition, one can find that the summation of the winding of $U_A(k)$ and $U_B(k)$ divided by 2 mode 1 leads to the polarization. This implies a relation between polarization and winding number in chiral-symmetric topological insulators: $p = \nu/2 \bmod 1$.

C. Winding number in real space

Recently, the winding number is generalized from momentum-space formula [Eq. (18)] to real-space formula [29,30,34]. The idea introduced in Ref. [29] is to replace the integral and the derivative versus quasimomentum k by its real-space representation. For a 1D system, the real-space winding number reads [29]

$$\nu = \mathcal{T}\{Q_{BA}[X, Q_{AB}]\}, \tag{20}$$

where $\mathcal{T}$ refers to trace per volume, $Q_{BA} = \Gamma_B Q \Gamma_A$, $Q_{AB} = \Gamma_A Q \Gamma_B$, and $\Gamma_\sigma = \sum_{l,\alpha\in\sigma} |l,\alpha\rangle\langle l,\alpha|$ is the projector onto the $\sigma = A, B$ subspaces [34]. The real-space formula is still valid even in the presence of disorder given that the chiral symmetry is preserved [29,30].

Here we present a quite different formula to calculate the winding number in real space. Later, we will prove that these two formulas are equivalent in the thermodynamic limit at half-filling. As stated in the previous section, the winding number is related to the relative polarization of A and B sublattice. We shall follow the projected position operator approach described in Sec. II to derive the winding number in real space.

To illustrate our idea, we consider a finite system with L cells and discretize the integral in Eq. (19) as

$$\nu = \frac{1}{2\pi i}\sum_k \mathrm{Tr}\Big[\log\Big(F_k^A F_k^{B^\dagger}\Big)\Big], \tag{21}$$

where $F_k^\sigma = U_\sigma^\dagger(k) U_\sigma(k-\delta k)$, $\sigma = A, B$, and $k = 2n\pi/L, n \in \mathbb{Z}$ (see Appendix A for a detailed derivation). Since the nth column of $U_\sigma(k)$ is the vector $|u_{n,k}^\sigma\rangle$, it can be found that the matrix elements of F_k^σ are $[F_k^\sigma]_{m,n} = \langle u_{m,k}^\sigma | u_{n,k-\delta k}^\sigma\rangle$.

Next, we propose the following equivalent formula to calculate the winding number:

$$\nu = \frac{1}{2\pi i}\mathrm{Tr}\big[\log\big(\mathcal{X}_A \mathcal{X}_B^{-1}\big)\big], \tag{22}$$

where $\mathcal{X}_\sigma = U_\sigma^{-1}\Gamma_\sigma \mathcal{X} \Gamma_\sigma U_\sigma$ ($\sigma = A, B$) are unitary matrices. $\mathcal{X}_\sigma$ can be considered as the position operator projected onto the σ sector of the eigenstate in the occupied band. The quantum-mechanical position operator can be chosen as

$$\mathcal{X} = \sum_{l,\alpha\in A,\beta\in B} e^{i\frac{2\pi}{L}l}(|l,\alpha\rangle\langle l,\alpha| + |l,\beta\rangle\langle l,\beta|). \tag{23}$$

Then this operator has the same form when it is projected to the A and B sectors. For convenience we denote the projected operators as $\tilde{\mathcal{X}} \equiv \Gamma_A \mathcal{X} \Gamma_A = \Gamma_B \mathcal{X} \Gamma_B$ in the following context.

To prove the equivalence between Eqs. (22) and (21), we note that

$$\begin{aligned}[\mathcal{X}_\sigma]_{(m,k'),(n,k)} &= \big\langle \psi_{m,k'}^\sigma \big| \mathcal{X} \big| \psi_{n,k}^\sigma \big\rangle \\ &= \delta_{k',k+\delta k}\big\langle u_{m,k'}^\sigma \big| u_{n,k}^\sigma \big\rangle,\end{aligned} \tag{24}$$

where $|\psi_{n,k}^\sigma\rangle = \sum_{\alpha\in\sigma} u_{n,k}^\sigma |k,\alpha\rangle$ is the σ sector of eigenstate (up to $1/\sqrt{2}$ normalization factor). Then we have

$$\begin{aligned}\big[\mathcal{X}_A \mathcal{X}_B^{-1}\big]_{(m,k'),(l,k'')} &= \sum_{n,k}[\mathcal{X}_A]_{(m,k'),(n,k)}\big[\mathcal{X}_B^{-1}\big]_{(n,k),(l,k'')} \\ &= \sum_{n,k}\delta_{k',k+\delta k}\delta_{k,k''-\delta k}\big\langle u_{m,k'}^A \big| u_{n,k}^A\big\rangle\big\langle u_{n,k}^B \big| u_{l,k''}^B\big\rangle \\ &= \delta_{k',k''}\sum_n \big\langle u_{m,k'}^A \big| u_{n,k'-\delta k}^A\big\rangle\big\langle u_{n,k''-\delta k}^B \big| u_{l,k''}^B\big\rangle \\ &= \delta_{k',k''}\sum_n \big[F_{k'}^A\big]_{m,n}\Big[\big(F_{k'}^B\big)^\dagger\Big]_{n,l}.\end{aligned} \tag{25}$$

Now we can see that matrix $\mathcal{X}_A\mathcal{X}_B^{-1}$ has a block-diagonal structure. Each block is associated with certain quasimomentum k, and is exactly equal to the matrix $F_k^A F_k^{B^\dagger}$. Therefore, one can immediately recognize that Eqs. (22) and (21) are equivalent.

Note that Eq. (21) should reproduce a strictly quantized winding number $\nu \in \mathbb{N}$. This can be proved by noting that $\det(\mathcal{X}_A\mathcal{X}_B^{-1}) = 1$, since U_σ and $\tilde{\mathcal{X}}$ are unitary matrices. Then, tracing the logarithm in Eq. (22) gives an integer multiple of $2\pi i$, and therefore the resulting winding number is an integer number.

We have to emphasize that this quantization occurs only when the system is half-filled, i.e., the Fermi energy lies in the band gap. Generally, when the Fermi surface lies in the bands (i.e., the filling is less than one half), the momentum-space winding number in Eq. (18) is ill-defined. However, the real-space formula (22) enables us to calculate the "winding number" at arbitrary fractional filling less than one half. As mentioned above, each column of U_σ is the σ sector of the eigenstates. Thus, one may select certain columns of U_σ to construct a reduced matrix $\tilde{U}_\sigma$, and then use Eq. (22) to calculate the winding number. Physically it can be understood as projecting the position operator onto a certain subspace. For example, we may choose the eigenstates whose energies are below the Fermi energy $E_n < E_F$ and calculate the corresponding fractional winding number via Eq. (22). As $\tilde{U}_\sigma$ is no

longer a unitary matrix after the reduction, the result may give a fractional value. We will verify this method numerically in Sec. IV B.

In addition, we shall show that our real-space representation of the winding number can be written in a form of the Bott index. By transforming $\mathcal{X}_A\mathcal{X}_B^{-1}$ via unitary matrix U_B and using $q = U_A U_B^{-1}$, we have

$$\begin{aligned} U_B\big(\mathcal{X}_A\mathcal{X}_B^{-1}\big)U_B^{-1} &= U_B\big(U_A^{-1}\tilde{\mathcal{X}}U_A U_B^{-1}\mathcal{X}^{-1}U_B\big)U_B^{-1} \\ &= \big(U_B U_A^{-1}\big)\tilde{\mathcal{X}}\big(U_A U_B^{-1}\big)\tilde{\mathcal{X}}^{-1} \\ &= q^{-1}\tilde{\mathcal{X}}q\tilde{\mathcal{X}}^{-1}. \end{aligned} \tag{26}$$

Hence, Eq. (22) can be written as

$$\begin{aligned} \nu &= \frac{1}{2\pi i}\mathrm{Tr}\log\left(q^{-1}\tilde{\mathcal{X}}q\tilde{\mathcal{X}}^{-1}\right) \\ &= \mathrm{Bott}(q^{-1},\tilde{\mathcal{X}}), \end{aligned} \tag{27}$$

which is exactly the form of Bott index introduced in [37,38]. In previous works, the Bott index is related to the real-space Chern number of the 2D topological insulator. To the best of our knowledge, the Bott index has not been applied to the real-space winding number of 1D chiral-symmetric topological insulators. Although the Bott indices for the Chern number and winding number have similar forms, they are fundamentally distinct.

D. Winding number defined through twisted boundary condition

In the previous subsection we obtain a real-space representation of the winding number for the 1D chiral-symmetric topological insulator. However, some of the properties, such as the self-averaging nature and the bulk-edge correspondence, are still vague. In this subsection we introduce the winding number defined through the twisted boundary condition (TBC). Then we prove the bulk-edge correspondence for the TBC winding number, which indicates that the TBC winding number is self-averaging in the presence of disorder in the thermodynamic limit. Next, we will prove that our real-space representation of winding number Eq. (22) is equivalent to the TBC winding number.

The TBC manifests that the two ends of the 1D lattice are glued together, but the particle will gain a phase Φ when they move through the boundary. Thus, the TBC is also called the generalized periodic boundary condition [43,44]. The TBC can be equivalently expressed as a result of the magnetic flux Φ piercing through the periodic chain. General 1D Hamiltonian under TBC can be written as

$$\begin{aligned} H(\Phi) &= -\sum_{\alpha,\beta,n\leqslant m} t_{m,n}^{\alpha,\beta} e^{i\Phi_{m,n}} c_{\alpha,m}^{\dagger} c_{\beta,n} + \mathrm{H.c.}, \\ \Phi_{m,n} &= \begin{cases} \Phi, & \langle m,n\rangle \text{ cross the boundary}, \\ 0, & \text{otherwise}. \end{cases} \end{aligned} \tag{28}$$

in which $c_{\alpha,m}^{\dagger}$ ($c_{\alpha,m}$) is the creation (annihilation) operator of the mth cell, α is the index of sublattice, and $t_{m,n}^{\alpha,\beta}$ is the corresponding tunneling strength.

1. Winding number and bulk-edge correspondence

The bulk-edge correspondence is a well-known principle in topological band theory. Nontrivial bulk topological invariant will lead to gapless excitations in the ground state at the edges. There have been some rigorous mathematical proofs of bulk-edge correspondence in the 1D chiral-symmetric topological insulator [45–47]. Here we use the TBC and follow the idea in Ref. [14] to derive this principle.

When the system possesses the chiral symmetry, as mentioned before, the flattened Hamiltonian is parametrized by the flux Φ,

$$Q(\Phi) = \begin{pmatrix} 0 & q(\Phi) \\ q^{-1}(\Phi) & 0 \end{pmatrix}. \tag{29}$$

In Ref. [48] it has been proved that the excitation gap will not be affected by the twist angle Φ in the thermodynamic limit. This means $q(\Phi)$ is nonsingular for arbitrary $\Phi \in [0, 2\pi]$ as long as the chiral-symmetric system is gapped at $E = 0$. Then, the TBC winding number can be safely defined as

$$\tilde{\nu} = \frac{1}{2\pi i}\int_0^{2\pi} d\Phi\ \mathrm{Tr}\big[q^{-1}(\Phi)\partial_\Phi q(\Phi)\big]. \tag{30}$$

Next, we show that the nontrivial winding number $\tilde{\nu} \neq 0$ under PBC results in the zero-energy modes, and the number of zero-energy modes is twice the winding number. Inspired by Ref. [14], we modify the boundary condition by adding a parameter $\eta \in [0, 1]$ onto the tunneling which crosses the boundary

$$t_{m,n}^{\alpha,\beta}(\eta) = \begin{cases} \eta t_{m,n}^{\alpha,\beta}, & \langle m,n\rangle \text{ cross the boundary}, \\ t_{m,n}^{\alpha,\beta}, & \text{otherwise}. \end{cases} \tag{31}$$

The system has open boundary when $\eta = 0$, and restores the usual TBC when $\eta = 1$. Now the Hamiltonian are parametrized by (Φ, η). Then we introduce the $U(1)$ phase field

$$z(\Phi,\eta) = \det q(\Phi,\eta) \in U(1). \tag{32}$$

Provided $z(\Phi, \eta) \neq 0$, the TBC winding number Eq. (30) can be written as

$$\tilde{\nu} = \frac{1}{2\pi i}\oint_{\eta=1} z^{-1}dz. \tag{33}$$

For nontrivial winding number $\tilde{\nu} \neq 0$, Eq. (33) implies some poles of z reside in the circle of $\eta = 1$, and the number of the poles should be equal to the absolute value of the winding number. Recall that the twist angle will not affect the excitation gap in the thermodynamic limit, the system should be either gapped or gapless at $E = 0$ for arbitrary twist angle $\Phi \in [0, 2\pi]$. This argument also holds for $\eta < 1$. Hence, there should be an infinite number of poles inside the circle if $z(\Phi, \eta) = 0$ for $0 < \eta < 1$, which is impossible when ν is well defined and the system is away from the phase transition. Consequently, the poles of $z(\Phi, \eta)$ can only occur at $\eta = 0$, which corresponds to the open boundary condition. This proof is similar to the discussion about the bulk-edge correspondence of the quantum Hall effect in Ref. [14].

Then we prove that the appearance of the zero-energy modes is associated to the nontrivial winding number. Note

that $z(\Phi,\eta)=\det q(\Phi,\eta)$ is proportional to the following products:

$$z(\Phi,\eta)=\det q(\Phi,\eta)\propto\prod_n \xi_n(\Phi,\eta), \tag{34}$$

in which $\{\xi_n(\Phi,\eta)\}$ are the singular values of $q(\Phi,\eta)$. We can learn from the above discussions that the number of poles is exactly equal to the number of zero singular values. Meanwhile, as mentioned in Sec. III A, the singular values of the off-diagonal block h are half of the eigenvalues of the corresponding chiral-symmetric Hamiltonian. Therefore, we can conclude that the number of zero-energy modes is twice the winding number under open boundary condition.

Since we have assumed the system is gapped under PBC, the zero-energy modes are the in-gap modes and should be localized at the edge, which is known as the bulk-edge correspondence. The above considerations are still valid if we replace the flattened Hamiltonian Q by the original Hamiltonian H. Importantly, this bulk-edge correspondence holds for the disordered case given that chiral symmetry persists. The bulk-edge correspondence also implies that the TBC winding number is self-averaging in the thermodynamic limit and away from the phase transition point.

2. *Equivalence of the TBC winding number and the real-space representation of the winding number*

Now we would like to prove that our real-space representation of winding number Eq. (22) is equivalent to the TBC winding number in the thermodynamic limit at half-filling. The TBC Hamiltonian (28) can be transformed to [48,49]

$$\begin{aligned}\tilde{H}(\Phi)&=\mathcal{U}_\Phi H(\Phi){\mathcal{U}_\Phi}^{-1}\\&=-\sum_{\alpha,\beta,n\leqslant m} t_{m,n}^{\alpha,\beta}e^{i\frac{\Phi}{L}(m-n)}c_{\alpha,m}^\dagger c_{\beta,n}+\text{H.c.},\end{aligned} \tag{35}$$

where

$$\mathcal{U}_\Phi=e^{i\frac{\Phi}{L}\hat{X}},\quad \hat{X}=\sum_{\alpha,m} m c_{\alpha,m}^\dagger c_{\alpha,m}. \tag{36}$$

We shall use the tilde notation to distinguish these two unitarily equivalent Hamiltonians in the following discussions. For a sufficiently large system $L\to\infty$, and assuming the range of tunneling is finite, we can expand Eq. (35) up to the leading order of Φ/L,

$$\begin{aligned}\tilde{H}(\Phi)&=H(0)+\frac{\Phi}{L}\mathcal{J}+O\left(\frac{1}{L^2}\right),\\ \mathcal{J}&=i\sum_{\alpha,\beta,n\leqslant m}\left[(m-n)t_{m,n}^{\alpha,\beta}c_{\alpha,m}^\dagger c_{\beta,n}-\text{H.c.}\right].\end{aligned} \tag{37}$$

One may notice that $\mathcal{J}$ is the current operator.

Similarly, we can expand $\tilde{q}(\Phi)$ up to the leading order of $\epsilon=\Phi/L$,

$$\tilde{q}(\epsilon)=q(0)+\epsilon[\partial_\epsilon\tilde{q}(\epsilon)]_{\epsilon=0}+O(\epsilon^2), \tag{38}$$

where we have expressed $\tilde{q}(\Phi)$ as $\tilde{q}(\epsilon)$ for clarity.

With this approximation, the winding number Eq. (30) can be written as

$$\begin{aligned}\nu&=\frac{1}{2\pi i}\int_0^{2\pi/L}d\epsilon\ \text{Tr}\left[\tilde{q}^{-1}(\epsilon)\partial_\epsilon\tilde{q}(\epsilon)\right]\\&=\frac{1}{2\pi i}\int_0^{2\pi/L}d\epsilon\ \text{Tr}\left\{q^{-1}(0)[\partial_\epsilon\tilde{q}(\epsilon)]_{\epsilon=0}\right\}+O(\epsilon^2)\\&=\frac{1}{iL}\text{Tr}\left\{q^{-1}(0)[\partial_\epsilon\tilde{q}(\epsilon)]_{\epsilon=0}\right\},\end{aligned} \tag{39}$$

where we have used the fact that $\{q^{-1}(0)[\partial_\epsilon\tilde{q}(\epsilon)]_{\epsilon=0}\}$ is independent on ϵ.

On the other hand, noting that $\mathcal{U}_{2\pi}=\mathcal{X}$, there is $H(0)=H(2\pi)=\mathcal{X}^{-1}\tilde{H}(2\pi)\mathcal{X}$ according to Eq. (35). This relation can be also generalized to the flattened Hamiltonian $Q(0)=\mathcal{X}^{-1}\tilde{Q}(2\pi)\mathcal{X}$. Since the matrix $q(\Phi)$ can be obtained from projecting the Q matrix via $\tilde{q}(\Phi)=\Gamma_A\tilde{Q}(\Phi)\Gamma_B$. We can derive a similar relation for the $q(0)$ and $\tilde{q}(2\pi)$,

$$\begin{aligned}q(0)&=\Gamma_A Q(0)\Gamma_B=\Gamma_A\mathcal{X}^{-1}\tilde{Q}(2\pi)\mathcal{X}\Gamma_B\\&=\left(\Gamma_A\mathcal{X}^{-1}\Gamma_A\right)\left[\Gamma_A\tilde{Q}(2\pi)\Gamma_B\right](\Gamma_B\mathcal{X}\Gamma_B)\\&=\tilde{\mathcal{X}}^{-1}\tilde{q}(2\pi)\tilde{\mathcal{X}},\end{aligned} \tag{40}$$

where we have used the fact that $\mathcal{X}$ is diagonal in the position space and $\Gamma_\sigma\mathcal{X}=\Gamma_\sigma\mathcal{X}\Gamma_\sigma$, $\Gamma_\sigma^2=\Gamma_\sigma$, $(\sigma=A,B)$.

Let $\epsilon=2\pi/L$ in Eq. (38), we can combine it with Eq. (40) and obtain the following relation:

$$\begin{aligned}\tilde{\mathcal{X}}q(0)\tilde{\mathcal{X}}^{-1}&=\tilde{q}\left(\epsilon=\frac{2\pi}{L}\right)\\&=q(0)+\frac{2\pi}{L}[\partial_\epsilon\tilde{q}(\epsilon)]_{\epsilon=0}+O\left(\frac{1}{L^2}\right).\end{aligned} \tag{41}$$

Therefore, we can rewrite Eq. (39) as

$$\begin{aligned}\nu&=\frac{1}{iL}\text{Tr}\left\{q^{-1}(0)[\partial_\epsilon\tilde{q}(\epsilon)]_{\epsilon=0}\right\}\\&=\frac{1}{2\pi i}\text{Tr}\left\{q^{-1}(0)\left[\tilde{\mathcal{X}}q(0)\tilde{\mathcal{X}}^{-1}-q(0)\right]\right\}\\&=\frac{1}{2\pi i}\text{Tr}\left(q^{-1}\tilde{\mathcal{X}}q\tilde{\mathcal{X}}^{-1}-I\right),\end{aligned} \tag{42}$$

where I is the identity matrix and we have dropped the dependence on the twist angle in the last row. From Eq. (41) one can find that $q^{-1}\tilde{\mathcal{X}}q\tilde{\mathcal{X}}^{-1}$ is close to the identity for sufficiently large L. In the thermodynamic limit $L\to\infty$, Eq. (42) can be written as the matrix logarithm [50]

$$\nu=\frac{1}{2\pi i}\text{Tr}\log\left(q^{-1}\tilde{\mathcal{X}}q\tilde{\mathcal{X}}^{-1}\right), \tag{43}$$

which is in agreement with Eq. (27). Thus, we have proved that the real-space representation of the winding number is equivalent to the winding number defined through the TBC in the thermodynamic limit at half-filling.

Generally speaking, to obtain the winding number defined through the TBC, one needs to change the twist angle Φ from 0 to 2π, which requires great computational resources. Here we have shown that the winding angle of $\tilde{q}(\Phi)$ changes linearly with the twist angle: $\arg[\det\tilde{q}(\Phi)]\sim\Phi$. It is such a kind of linear dependence that leads to our efficient real-space representation of the winding number. Moreover, as discussed

above, the TBC winding number should be a self-averaging quantity, and we can therefore conclude that our real-space representation of the winding number is also self-averaging.

In addition, we can further prove that the TBC winding number [Eq. (30)], as well as the real-space representation of the winding number [Eq. (22)] in our work, are equivalent to the formula [Eq. (20)] obtained in Ref. [29]. To show this, we note that in the thermodynamic limit, there is

$$\begin{aligned}[X, H(0)] &= \sum_{\alpha,\beta,n\leqslant m} \left[(m-n)t^{\alpha,\beta}_{m,n} c^{\dagger}_{\alpha,m} c_{\beta,n} - \text{H.c.}\right] \\ &= -i\mathcal{J}, \end{aligned} \tag{44}$$

where $X = \sum_{\alpha,m} m c^{\dagger}_{\alpha,m} c_{\alpha,m}$. On the other hand, the off-diagonal block $h(\Phi)$ matrix and its inverse read as

$$\tilde{h}(\Phi) = \Gamma_A \tilde{H}(\Phi)\Gamma_B, \quad \tilde{h}(\Phi)^{-1} = \Gamma_B \tilde{H}(\Phi)^{-1}\Gamma_A. \tag{45}$$

Hence, using Eq. (37), the derivative with respect to Φ reads as

$$\begin{aligned}\left[\partial_\epsilon \tilde{h}(\epsilon)\right]_{\epsilon=0} &= L\left[\partial_\Phi \tilde{h}(\Phi)\right]_{\Phi=0} \\ &= \Gamma_A \mathcal{J} \Gamma_B \\ &= i\Gamma_A [X, H(0)]\Gamma_B. \end{aligned} \tag{46}$$

The winding number [Eq. (39)] can be equivalently written as

$$\tilde{\nu} = \frac{1}{iL} h(0)^{-1}\left[\partial_\epsilon \tilde{h}(\epsilon)\right]_{\epsilon=0} = \frac{1}{L}\Gamma_B H^{-1}\Gamma_A [X, H]\Gamma_B, \tag{47}$$

where we have dropped the dependence on the twist angle Φ in the last term for simplicity. Then, it is tempting to replace the Hamiltonian by the flattened Hamiltonian, and we have

$$\begin{aligned}\tilde{\nu} &= \frac{1}{L}\Gamma_B Q \Gamma_A [X, Q]\Gamma_B \\ &= \frac{1}{L} Q_{BA}[X, Q_{AB}], \end{aligned} \tag{48}$$

in which we have used the relation $\Gamma_\sigma^2 = \Gamma_\sigma$, $\Gamma_\sigma X = \Gamma_\sigma X \Gamma_\sigma$ ($\sigma = A, B$), and $Q^{-1} = Q$. We find that Eq. (48) is identical to Eq. (20). Therefore, we can conclude that the TBC winding number [Eq. (30)], the real-space representation of the winding number [Eq. (22)] in our work, and the real-space formula [Eq. (20)] obtained in Ref. [29], are equivalent in the thermodynamic limit. Note that Eq. (48) can be also derived from Eq. (42) by using the Baker-Campbell-Hausdorff formula to expand $\tilde{\mathcal{X}} q \tilde{\mathcal{X}}^{-1}$ up to the first term, but the convergence of the expansion seems to be unclear in that way.

E. Winding number defined through path connection

Previously we obtain the real-space winding number by considering the sublattice polarization. We find that our formula can be expressed as the Bott index. For the Bott index there is an alternative method to express the winding number by a path connection [37], which clearly shows the meaning of winding in real space. We shall give a simple illustration here.

Since unitary matrix is always diagonalizable, we can make an eigenvalue decomposition $\mathcal{X}_A \mathcal{X}_B^{-1} = T\mathcal{X}_{\text{diag}} T^{-1}$ where T is an unitary matrix and $\mathcal{X}_{\text{diag}} = \text{diag}\{e^{i\theta_1}, e^{i\theta_2}, \ldots, e^{i\theta_n}\}$ is a diagonal matrix with all elements lying on an unit circle in complex plane $\mathbb{C}$.

Then Eq. (22) can be written as

$$\nu = \frac{1}{2\pi i}\text{Tr}[\log(\mathcal{X}_{\text{diag}})] = \frac{1}{2\pi}\sum_k \theta_k. \tag{49}$$

In other words, the information of the winding number is encoded in these phases.

Recall that the matrix logarithm is a multivalued matrix function. To "unwind" the logarithm in Eq. (22), we consider a continuous path (homotopy) $\phi : [0, 1] \to \text{GL}(n, \mathbb{C})$ such that $\phi(0) = \mathcal{X}_A \mathcal{X}_B^{-1}$ and $\phi(1) = I$. The function $\phi(r)$ can be written as

$$\begin{aligned}\phi(r) &= T\mathcal{X}_{\text{diag}}(r) T^{-1} \\ &= T\,\text{diag}\left\{e^{i\tilde{\theta}_1(r)}, e^{i\tilde{\theta}_2(r)}, \ldots, e^{i\tilde{\theta}_n(r)}\right\} T^{-1}, \end{aligned} \tag{50}$$

where $\tilde{\theta}_k(r) \in [0, 2\pi)$, $r \in [0, 1]$ is a continuous real function with $\tilde{\theta}_k(0) = \theta_k$ and $\tilde{\theta}_k(1) = 0$. The winding number can be defined as

$$\nu = -\frac{1}{2\pi}\int_0^1 dr \frac{\partial}{\partial r} \arg[\det \phi(r)], \tag{51}$$

which is indeed related to the real-space winding number since

$$\begin{aligned}&-\frac{1}{2\pi}\int_0^1 dr \frac{\partial}{\partial r} \arg[\det \phi(r)] \\ &\quad = -\frac{1}{2\pi}\sum_k \int_0^1 dr \frac{\partial}{\partial r}\tilde{\theta}_k(r) = \frac{1}{2\pi}\sum_k \theta_k, \end{aligned} \tag{52}$$

where we have used $\int_0^1 dr \frac{\partial}{\partial r}\tilde{\theta}_k(r) = -\theta_k$.

When the winding number is nontrivial $\nu > 0$, the continuous path ϕ connects different branches of a complex logarithm. The winding number can only be changed discontinuously when the system undergoes a phase transition. This is accompanied by the sudden changes of some phase θ_k, and the function $\arg[\det \phi(r)]$ becomes discontinuous and indifferentiable. Note that $\det \phi(r)$ may be still continuous and well defined. The singularity of $\arg[\det \phi(r)]$ is due to the multivalued nature of the argument. For example, when a phase grows continuously from θ_0 to $\theta_0 + 2\pi$, the complex function $e^{i\theta_0}$ is continuous, while its principal argument $\arg(e^{i\theta_0})$ is discontinuous. We will show this later with a numerical calculation.

In the presence of translation symmetry, we have proved that our formula (22) is exactly equal to the momentum-space formula (18). Thus, it is natural that the winding number [Eq. (51)] is also equivalent to the momentum-space formula [Eq. (18)]. Also, it is always possible to elaborate a path that the behavior of the winding number defined in Eq. (51) is identical to the momentum-space winding number [Eq. (18)] when translation symmetry is present. In other words, the loop $\det \phi(r)$ is homotopic to $\det h(k)$ and $\det q(k)$ in the presence of translation symmetry.

IV. APPLICATION TO A 1D BDI CLASS MODEL

In the previous section we have introduced a representation of the real-space winding number. Our formula ensures that the winding number is an integer at half-filling case. For arbitrary fractional filling less than one half, our formula is still

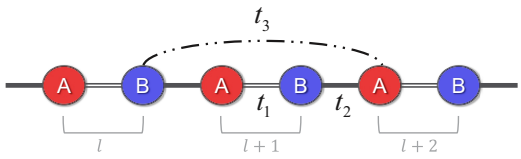

FIG. 1. Schematic illustration of the extended SSH model. Besides the general nearest-neighbor tunneling in the SSH model, we include special long-range tunneling indicated by the dashed line.

applicable but does not necessarily give an integer number. On the other hand, we define a winding number through a continuous path from the special unitary matrix to the identity matrix. In this section we will apply these arguments to a toy model in the 1D BDI class. We shall also consider a disorder on tunneling to see the robustness and validity of the real-space winding number. These calculations can be easily extended to the AIII class.

A. Extended Su-Schrieffer-Heeger model and disordered tunneling

We introduce a 1D lattice model described by the following second quantized Hamiltonian:

$$H = -\sum_l \left(t_{1,l}\hat{a}_l^\dagger \hat{b}_l + t_{2,l}\hat{a}_{l+1}^\dagger \hat{b}_l + t_{3,l}\hat{a}_{l+2}^\dagger \hat{b}_l\right) + \text{H.c.}, \quad (53)$$

where $\hat{a}_l{}^\dagger$ ($\hat{b}_l{}^\dagger$) creates a particle at the A (B) sublattice of the lth cell. $t_{n,l} = t_n + W_n\varepsilon_{n,l}$, $n = 1, 2, 3$ is the tunneling strength, $\varepsilon_{n,l} \in (-1/2, 1/2)$ is a random strength distributed uniformly, and W_n is the strength of disorder. This is an extended Su-Schrieffer-Heeger (SSH) model up to a next-next-nearest-neighbor (NNNN) term. A schematic illustration of this toy model is shown in Fig. 1. With this special NNNN tunneling, the system still preserves chiral symmetry. According to the tenfold classification, this model belongs to BDI class. There exist topological phases characterized by winding number $\nu = 0, 1, 2$ in this model.

As a benchmark, we adapt a similar configuration in Ref. [30], and set $W = W_1 = 2W_2$, $W_3 = 0$ and $t_1 = 0, t_2 = 1, t_3 = -2$. We use the two approaches Eqs. (20) and (22) to numerically calculate the winding number as a function of disorder strength W. Here the position operator reads as $\hat{\mathcal{X}} = \exp[i\delta k \sum_i l(\hat{a}_l^\dagger \hat{a}_l + \hat{b}_l^\dagger \hat{b}_l)]$. The results are shown in Fig. 2. It can be seen that the winding numbers obtained from Eq. (22) stay quantized in each random realization (gray dots). We have examined that the averaged results (blue circles) agree well with the averaged results obtained from Eq. (20). Away from the phase transition point, there is almost no fluctuation of the winding number because each realization is perfectly the same quantization. Around the phase transition point we find that the fluctuation of winding number becomes large, which can be served as a signature of the topological phase transition in disorder systems. The phase transition point can be determined with higher accuracy as the lattice length increases. The scaling with different lattice lengths is presented in Appendix. B. However, we note that the real-space winding number obtained from Eq. (20) is not strictly quantized for the finite system. As shown in the inset of Fig. 2, the real-space

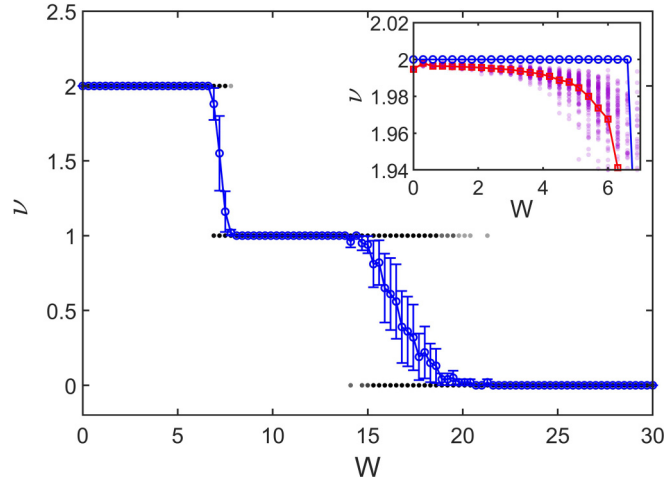

FIG. 2. Winding number ν as a function of disorder strength W in disordered extended SSH model in Eq. (53). Gray dots are the results from 100 random realizations based on Eq. (22). Blue circles are averaged over the gray dots. Inset: Comparison between Eqs. (20) and (22). Light-purple dots are the results from 100 random realization based on Eq. (20). Red squares are the averaged results of the purple dots. The above calculations are implemented with $L = 1001$ cells. The parameters are $t_1 = 0, t_2 = 1, t_3 = -2$, and the configuration of disorder is $W = W_1 = 2W_2, W_3 = 0$.

winding number calculated via Eq. (20) slightly deviates from the integer.

Next, based on Eq. (51), we use Eq. (51) to graphically show the winding number in the presence of disorder. Practically we can simply assume

$$\phi(r) = (1-r)\mathcal{X}_A\mathcal{X}_B^{-1} + rI, \quad r \in [0, 1]. \quad (54)$$

The determinant is

$$\begin{aligned}\det\phi(r) &= \det\left[(1-r)\mathcal{X}_A\mathcal{X}_B^{-1} + rI\right] \\ &= \det\left\{T[(1-r)\mathcal{X}_{\text{diag}} + rI]T^{-1}\right\} \\ &= \det\left[(1-r)\mathcal{X}_{\text{diag}} + rI\right] \\ &= \prod_k \left[(1-r)e^{i\theta_k} + r\right].\end{aligned} \quad (55)$$

The graphical illustrations of real-space winding numbers are shown in Figs. 3(a)–3(c). It can be seen that the winding around the singularity point [$\det\phi(r) = 0$] in the complex plane coincides well with the real-space winding number.

Besides, it can be found that $\det\phi(r)$ only takes zero value at $r = 1/2$ and $\theta_k = \pi$. As stated in the previous section, we may identify that $\theta_k = \pi$ is related to the discontinuous change of argument, and thus corresponds to phase transition. To show this, we numerically calculate the arguments $\{\theta_k\}$ from the diagonal entries of X_{diag} as a function of disorder strength W in a *single* random realization $\{\varepsilon_{n,l}\}$. As presented in Figs. 3(d) and 3(e), given a random realization $\{\varepsilon_{n,l}\}$, all the phases $\{\theta_k\}$ change continuously with disorder strength except for the phase transition point. This is in agreement with our discussion.

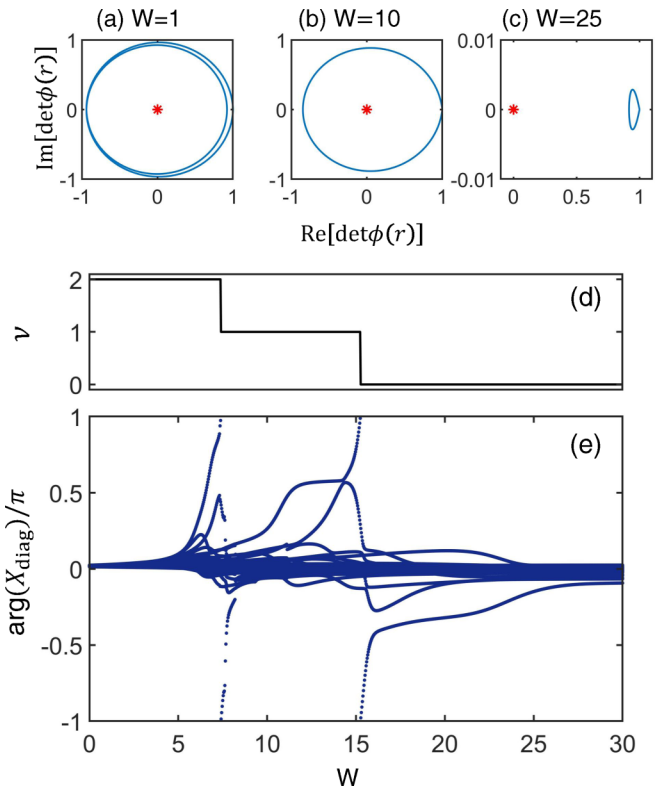

FIG. 3. (a)–(c) The trajectory of $\det \phi(r)$ with $W = 1, 10, 25$ in a single random realization. The red star represents the zero point. (d) The real-space winding number ν as a function of disorder strength W given a certain set of random factor $\{\varepsilon_{n,l}\}$ in a single random realization. (e) The argument $\{\theta_k\}$ of the diagonal entries of $\mathcal{X}_{\text{diag}}$ as a function of W in the same random realization as (d). Other parameters are identical to the parameters in Fig. 2.

B. Winding number under different filling factors

Now we calculate the winding number for various fillings (less than one half) in the extended SSH model; see Fig. 4. It can be seen that the winding number is zero when the filling is empty. As the Fermi energy increases, the winding number changes continuously, and finally reaches an integer value when the system is half-filled (the Fermi energy E_{F} lies in the spectral gap). This result may be understood by considering the winding number as the difference of polarization of A and B sublattices. The difference in sublattice polarization will change with the filling numbers.

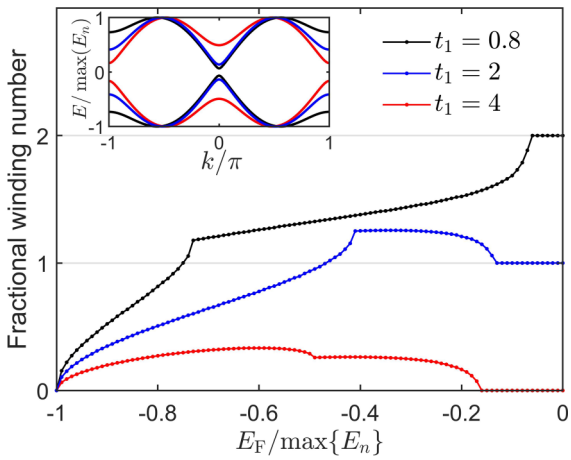

FIG. 4. Winding number as a function of Fermi energy E_F for three different parameters $t_1 = 0.8, 2, 4$ in the clean limit $W_1 = W_2 = W_3 = 0$. The inset shows the corresponding band structure. Other parameters are chosen as $t_2 = 1, t_3 = -2$.

Notice that there appears discontinuity in the first derivative of the Fermi energy. This is because there are some local minima in the band structure, as shown in the inset of Fig. 4. This method can be also applied to the disordered case.

V. SUMMARY AND DISCUSSION

In summary, we propose a real-space formula for calculating the winding number of 1D chiral-symmetric systems. Our real-space representation of the winding number is inspired by the projected position operator approach since the winding number can be written as the difference of polarization between two sublattices. We show that our approach is equivalent to the momentum-space representation of the winding number in the clean limit. Even in the presence of disorder, our formula produces a quantized value. We have also shown that our method works for the case of fillings less than one half.

With the help of TBC, we have proved the bulk-edge correspondence principle for the TBC winding number. We further prove that our real-space representation of winding number is equivalent to the TBC winding number and the real-space formula proposed in Ref. [29] in the thermodynamic limit at half-filling. Therefore our real-space representation of winding number also satisfies the bulk-edge correspondence and the self-averaging property. Meanwhile, compared with the general TBC method, where includes the integral of twist angle Φ, our formula can be obtained from a single Hamiltonian, which is more efficient.

Interestingly, we find that our real-space winding number can be expressed as a Bott index. However, the Bott index is usually employed for the real-space Chern number [19,51,52], which is quite different from the winding number in a 1D chiral-symmetric topological insulator. We also show that the Bott index has a deep connection to the twisted boundary condition. Our work may provide another concrete example for investigating the Bott index. Meanwhile, one may find the position operator plays a crucial role in the construction of real-space representation of topological invariants, such as the Chern number [16–20], the Zak-Berry phase [25–28], and the winding number [29–35]. Thus, it is intriguing to generalize the application of position operators to other topological systems in other topological classes or higher dimension in the future.

We also note that recently the SVD has been applied to non-Hermitian systems [53], where the singular values of a non-Hermitian Hamiltonian obey the bulk-edge correspondence. The study on the interplay between non-Hermitian systems and disorder has received many interests recently [54,55]. With the formula of winding number for the non-Hermitian system [56], it is intriguing to generalize our formula to the non-Hermitian case. The non-Hermitian

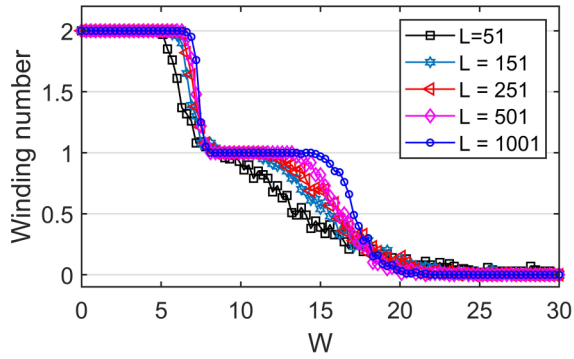

FIG. 5. Winding number as a function of disorder strength W with different length L of system. The results are averaged over 100 random realizations. Other parameters are the same as Fig. 2.

Hamiltonian can be considered as the off-diagonal block of some chiral-symmetric Hermitian Hamiltonians. Then our real-space representation of the winding number may be extended to non-Hermitian systems.

ACKNOWLEDGMENTS

This work has been supported by the National Natural Science Foundation of China (12025509, 11874434), the Key-Area Research and Development Program of Guangdong Province (2019B030330001), and the Science and Technology Program of Guangzhou (201904020024). Y.K. is partially supported by the National Natural Science Foundation of China (Grant No. 11904419).

APPENDIX A: DERIVATION OF THE DISCRETIZED FORMULA OF THE WINDING NUMBER

Here we give a detailed derivation of Eq. (21). Approximately we have

$$U_\sigma^{-1}(k)\partial_k U_\sigma(k) \simeq U_\sigma^{-1}(k)\frac{U_\sigma(k+\delta k)-U_\sigma(k)}{\delta k}, \tag{A1}$$

which leads to

$$1 + U_\sigma^{-1}(k)\partial_k U_\sigma(k)\delta k \simeq U_\sigma^{-1}(k)U_\sigma(k+\delta k). \tag{A2}$$

Take the logarithm on both sides

$$\log\left[1 + U_\sigma^{-1}(k)\partial_k U_\sigma(k)\delta k\right] \simeq \log\left[U_\sigma^{-1}(k)U_\sigma(k+\delta k)\right], \tag{A3}$$

and use the approximation $\log(1+x) \approx x$ when $x \to 0$, we obtain

$$U_\sigma^{-1}(k)\partial_k U_\sigma(k)\delta k \simeq \log\left[U_\sigma^{-1}(k)U_\sigma(k+\delta k)\right]. \tag{A4}$$

In the thermodynamic limit, the quantities in two sides of Eq. (A4) are equivalent. Thus, the discretized form of winding number can be written as

$$\nu = \frac{1}{2\pi i}\sum_k \mathrm{Tr}\left(\log F_k^A - \log F_k^B\right), \tag{A5}$$

where $F_k^\sigma = U_\sigma^\dagger(k)U_\sigma(k-\delta k)$, $\sigma = A, B$. Alternatively, we can use the fact that $\mathrm{Tr}\log(A) = \log\det(A)$ when $\|A\| < \pi$ [57], and then obtain the expression in Eq. (21).

APPENDIX B: SCALING OF THE PHASE TRANSITION

To examine the finite-size effect on the disorder-induced topological phase transition, we present the winding number as a function of disorder strength W in Fig. 5. The results show that the boundary of phase transition tends to be clear when $L \to \infty$.

[1] C. L. Kane, Topological band theory and the $\mathbb{Z}_2$ invariant, Contemp. Concept Conden. Matter Sci. **6**, 3 (2013).
[2] F. D. M. Haldane, Model for a Quantum Hall Effect without Landau Levels: Condensed-Matter Realization of the "Parity Anomaly", Phys. Rev. Lett. **61**, 2015 (1988).
[3] C. L. Kane and E. J. Mele, Quantum Spin Hall Effect in Graphene, Phys. Rev. Lett. **95**, 226801 (2005).
[4] B. A. Bernevig, T. L. Hughes, and S.-C. Zhang, Quantum spin Hall effect and topological phase transition in HgTe quantum wells, Science **314**, 1757 (2006).
[5] B. A. Bernevig and S.-C. Zhang, Quantum Spin Hall Effect, Phys. Rev. Lett. **96**, 106802 (2006).
[6] K. v. Klitzing, G. Dorda, and M. Pepper, New Method for High-Accuracy Determination of the Fine-Structure Constant Based on Quantized Hall Resistance, Phys. Rev. Lett. **45**, 494 (1980).
[7] D. J. Thouless, M. Kohmoto, M. P. Nightingale, and M. den Nijs, Quantized Hall Conductance in a Two-Dimensional Periodic Potential, Phys. Rev. Lett. **49**, 405 (1982).
[8] B. A. Bernevig and T. L. Hughes, *Topological Insulators and Topological Superconductors* (Princeton University Press, Princeton, NJ, 2013).
[9] L. Fu, C. L. Kane, and E. J. Mele, Topological Insulators in Three Dimensions, Phys. Rev. Lett. **98**, 106803 (2007).
[10] K. Nomura and N. Nagaosa, Surface-Quantized Anomalous Hall Current and the Magnetoelectric Effect in Magnetically Disordered Topological Insulators, Phys. Rev. Lett. **106**, 166802 (2011).
[11] L. Sheng, D. N. Sheng, C. S. Ting, and F. D. M. Haldane, Nondissipative Spin Hall Effect via Quantized Edge Transport, Phys. Rev. Lett. **95**, 136602 (2005).
[12] C. Xu and J. E. Moore, Stability of the quantum spin Hall effect: Effects of interactions, disorder, and $\mathbb{Z}_2$ topology, Phys. Rev. B **73**, 045322 (2006).
[13] C. Wu, B. A. Bernevig, and S.-C. Zhang, Helical Liquid and the Edge of Quantum Spin Hall Systems, Phys. Rev. Lett. **96**, 106401 (2006).

[14] X.-L. Qi, Y.-S. Wu, and S.-C. Zhang, General theorem relating the bulk topological number to edge states in two-dimensional insulators, Phys. Rev. B **74**, 045125 (2006).

[15] K. Kobayashi, T. Ohtsuki, and K.-I. Imura, Disordered Weak and Strong Topological Insulators, Phys. Rev. Lett. **110**, 236803 (2013).

[16] E. Prodan, T. L. Hughes, and B. A. Bernevig, Entanglement Spectrum of a Disordered Topological Chern Insulator, Phys. Rev. Lett. **105**, 115501 (2010).

[17] E. Prodan, Disordered topological insulators: A non-commutative geometry perspective, J. Phys. A: Math. Theor. **44**, 113001 (2011).

[18] R. Bianco and R. Resta, Mapping topological order in coordinate space, Phys. Rev. B **84**, 241106(R) (2011).

[19] T. A. Loring and M. B. Hastings, Disordered topological insulators via C^*-algebras, Europhys. Lett. **92**, 67004 (2010).

[20] Z. Yi-Fu, Y. Yun-You, J. Yan, S. Li, S. Rui, S. Dong-Ning, and X. Ding-Yu, Coupling-matrix approach to the Chern number calculation in disordered systems, Chin. Phys. B **22**, 117312 (2013).

[21] M. A. Bandres, M. C. Rechtsman, and M. Segev, Topological Photonic Quasicrystals: Fractal Topological Spectrum and Protected Transport, Phys. Rev. X **6**, 011016 (2016).

[22] D. F. Mross, Y. Oreg, A. Stern, G. Margalit, and M. Heiblum, Theory of Disorder-Induced Half-Integer Thermal Hall Conductance, Phys. Rev. Lett. **121**, 026801 (2018).

[23] T. A. Loring, K-theory and pseudospectra for topological insulators, Ann. Phys. **356**, 383 (2015).

[24] Y. Xue and E. Prodan, Noncommutative Kubo formula: Applications to transport in disordered topological insulators with and without magnetic fields, Phys. Rev. B **86**, 155445 (2012).

[25] S. Kivelson, Wannier functions in one-dimensional disordered systems: Application to fractionally charged solitons, Phys. Rev. B **26**, 4269 (1982).

[26] Q. Niu, Theory of the quantized adiabatic particle transport, Mod. Phys. Lett. B **5**, 923 (1991).

[27] N. Marzari, A. A. Mostofi, J. R. Yates, I. Souza, and D. Vanderbilt, Maximally localized Wannier functions: Theory and applications, Rev. Mod. Phys. **84**, 1419 (2012).

[28] W. A. Benalcazar, B. A. Bernevig, and T. L. Hughes, Electric multipole moments, topological multipole moment pumping, and chiral hinge states in crystalline insulators, Phys. Rev. B **96**, 245115 (2017).

[29] I. Mondragon-Shem, T. L. Hughes, J. Song, and E. Prodan, Topological Criticality in the Chiral-Symmetric AIII Class at Strong Disorder, Phys. Rev. Lett. **113**, 046802 (2014).

[30] J. Song and E. Prodan, AIII and BDI topological systems at strong disorder, Phys. Rev. B **89**, 224203 (2014).

[31] C.-B. Hua, R. Chen, D.-H. Xu, and B. Zhou, Disorder-induced Majorana zero modes in a dimerized Kitaev superconductor chain, Phys. Rev. B **100**, 205302 (2019).

[32] J. Claes and T. L. Hughes, Disorder driven phase transitions in weak AIII topological insulators, Phys. Rev. B **101**, 224201 (2020).

[33] L. Lin, S. Kruk, Y. Ke, C. Lee, and Y. Kivshar, Topological states in disordered arrays of dielectric nanoparticles, Phys. Rev. Research **2**, 043233 (2020).

[34] E. J. Meier, F. A. An, A. Dauphin, M. Maffei, P. Massignan, T. L. Hughes, and B. Gadway, Observation of the topological Anderson insulator in disordered atomic wires, Science **362**, 929 (2018).

[35] M. Maffei, A. Dauphin, F. Cardano, M. Lewenstein, and P. Massignan, Topological characterization of chiral models through their long time dynamics, New J. Phys. **20**, 013023 (2018).

[36] C.-K. Chiu, J. C. Y. Teo, A. P. Schnyder, and S. Ryu, Classification of topological quantum matter with symmetries, Rev. Mod. Phys. **88**, 035005 (2016).

[37] R. Exel and T. A. Loring, Invariants of almost commuting unitaries, J. Funct. Anal. **95**, 364 (1991).

[38] M. B. Hastings and T. A. Loring, Almost commuting matrices, localized Wannier functions, and the quantum Hall effect, J. Math. Phys. **51**, 015214 (2010).

[39] R. Resta, Quantum-Mechanical Position Operator in Extended Systems, Phys. Rev. Lett. **80**, 1800 (1998).

[40] N. Marzari and D. Vanderbilt, Maximally localized generalized Wannier functions for composite energy bands, Phys. Rev. B **56**, 12847 (1997).

[41] A. Alexandradinata, Z. Wang, and B. A. Bernevig, Topological Insulators from Group Cohomology, Phys. Rev. X **6**, 021008 (2016).

[42] S. Ryu, A. P. Schnyder, A. Furusaki, and A. W. Ludwig, Topological insulators and superconductors: tenfold way and dimensional hierarchy, New J. Phys. **12**, 065010 (2010).

[43] Q. Niu and D. J. Thouless, Quantised adiabatic charge transport in the presence of substrate disorder and many-body interaction, J. Phys. A: Math. Gen. **17**, 2453 (1984).

[44] Q. Niu, D. J. Thouless, and Y.-S. Wu, Quantized Hall conductance as a topological invariant, Phys. Rev. B **31**, 3372 (1985).

[45] C. L. Kane, in *Topological Insulators*, Contemporary Concepts of Condensed Matter Science, edited by M. Franz and L. Molenkamp (Elsevier, 2013), Vol. 6, pp. 3–34.

[46] G. M. Graf and J. Shapiro, The bulk-edge correspondence for disordered chiral chains, Commun. Math. Phys. **363**, 829 (2018).

[47] J. Shapiro, The bulk-edge correspondence in three simple cases, Rev. Math. Phys. **32**, 2030003 (2020).

[48] H. Watanabe, Insensitivity of bulk properties to the twisted boundary condition, Phys. Rev. B **98**, 155137 (2018).

[49] H. Watanabe and M. Oshikawa, Inequivalent Berry Phases for the Bulk Polarization, Phys. Rev. X **8**, 021065 (2018).

[50] N. J. Higham, *Functions of Matrices: Theory and Computation* (SIAM, Philadelphia, PA, 2008).

[51] T. A. Loring, Quantitative K-theory related to spin Chern numbers, Symmetry, Integrability Geom.: Methods Appl. (SIGMA) **10**, 077 (2014).

[52] D. Toniolo, On the equivalence of the Bott index and the Chern number on a torus, and the quantization of the Hall conductivity with a real space Kubo formula, arXiv:1708.05912.

[53] L. Herviou, J. H. Bardarson, and N. Regnault, Defining a bulk-edge correspondence for non-Hermitian Hamiltonians via singular-value decomposition, Phys. Rev. A **99**, 052118 (2019).

[54] S. Velury, B. Bradlyn, and T. L. Hughes, Topological crystalline phases in a disordered inversion-symmetric chain, Phys. Rev. B **103**, 024205 (2021).

[55] J. Claes and T. L. Hughes, Skin effect and winding number in disordered non-Hermitian systems, Phys. Rev. B **103**, L140201 (2021).

[56] Z. Gong, Y. Ashida, K. Kawabata, K. Takasan, S. Higashikawa, and M. Ueda, Topological Phases of Non-Hermitian Systems, Phys. Rev. X **8**, 031079 (2018).

[57] M. Aprahamian and N. J. Higham, The matrix unwinding function, with an application to computing the matrix exponential, SIAM J. Matrix Anal. Appl. **35**, 88 (2014).